


Characteristics of compact stars determined by gravitational waves, radio-astronomy, x-ray emission, and nuclear physics

H. Güven 

*Université Paris-Saclay, CNRS/IN2P3, IJCLab, 91405 Orsay, France
and Physics Department, Yildiz Technical University, 34220 Esenler, Istanbul, Turkey*

J. Margueron 

Université Lyon, Université Claude Bernard Lyon 1, CNRS/IN2P3, IP2I Lyon, UMR 5822, F-69622, Villeurbanne, France

K. Bozkurt 

*Physics Department, Yildiz Technical University, 34220 Esenler, Istanbul, Turkey
and Université Paris-Saclay, CNRS/IN2P3, IJCLab, 91405 Orsay, France*

E. Khan 

Université Paris-Saclay, CNRS/IN2P3, IJCLab, 91405 Orsay, France



(Received 5 April 2023; revised 26 July 2023; accepted 30 August 2023; published 25 September 2023)

We investigate the question of the nature of compact stars, considering they may be neutron stars or hybrid stars containing a quark core, within the present constraints given by gravitational waves, radio-astronomy, x-ray emissions from millisecond pulsars and nuclear physics. A Bayesian framework is used to combine together all these constraints and to predict tidal deformabilities and radii for a $1.4 M_{\odot}$ compact star. We find that present gravitation wave and radioastronomy data favor stiff nucleonic equation of state (EoS) compatible with nuclear physics and that GW170817 waveform is best described for binary hybrid stars. Binary neutron stars with soft EoS could however not be totally excluded. In all cases, these data favor stiff quark matter, independently of the nuclear EoS, with a low value for the transition density ($n_{tr} \in [0.18, 0.35] \text{ fm}^{-3}$). Combining these results with constraints from x-ray observation supports the existence $1.4 M_{\odot}$ mass hybrid star, with a radius predicted to be about $R_{1.4} = 12.22(45) \text{ km}$.

DOI: [10.1103/PhysRevC.108.035810](https://doi.org/10.1103/PhysRevC.108.035810)

I. INTRODUCTION

Neutron stars (NSs), and most generally compact stars (CSs), are forefront laboratories to explore the properties of extreme matter and consequently the strong interaction. The guidance of experimental and observational data are of prime importance, especially because the theory of strong interaction, the quantum chromodynamics (QCD), could not be simply applied in the regime explored by CSs. One of the most important questions in this field is to understand how the strong interaction evolves as function of the density and how quark matter emerges from hadrons [1,2], if it ever does for densities relevant for stable CSs. Therefore, one should consider two types of CS: NS with no phase transition in the core, and hybrid stars (HS) with phase transition, towards quark matter, in the core. Note that the existence of strange quark stars is not considered in our analysis since we assume that matter is ruled by a single equation of state. In the present paper, we investigate the onset of a first order phase transition (FOPT) producing the largest correction to the global properties of CSs. It should be noted that CSs observations are also complementary to Earth experiments, such as for instance heavy ion collision

[3], since they explore very isospin asymmetric and dense matter.

Over the last decade, the observation of CSs has entered into the era of precision measurements, which provides unprecedented possibilities for constraining the equation of state (EoS). Among these constraints, the most impactful ones are shown in Fig. 1: The detection of massive NSs by radio astronomers has pushed up the maximum mass limit, which is presently around $2M_{\odot}$ [6,10–14]. As a typical example, the maximum mass limit from J0348 + 0432 [6] is shown in Fig. 1. In addition to the masses, the radii of a few millisecond pulsars (PSR J0030 + 0451 [7,15] and PSR-J0740 + 6620 [8,16]) have recently been extracted from x-ray observations, using the NICER observatory [17]. Finally, the event GW170817 [18–20], produced by the merger of two CSs, allowed the first estimation of the effective tidal deformability $\tilde{\Lambda}$ for dense matter [21–23], which is shown in the right panels in Fig. 1.

II. THEORY

The link between the observation of CSs and the strong interaction is performed through the EoS, i.e., the pressure

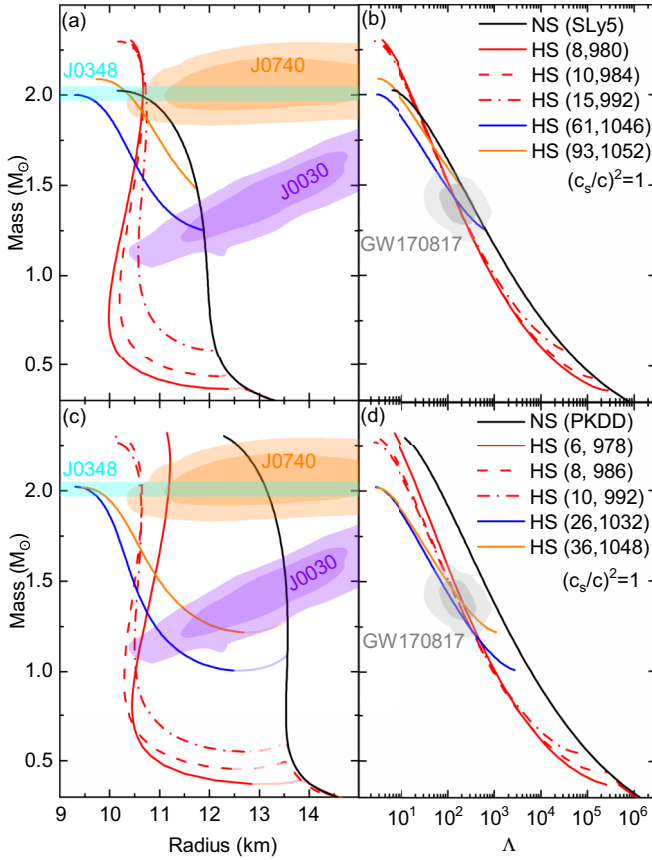


FIG. 1. Mass-radius (left) and mass-tidal deformability (right) representations for SLy5 [4] (top) and PKDD [5] (bottom). The observational contours are related to the analysis of J0348 + 0432 [6], J0030 + 0451 [7], J0740 + 6620 [8], and GW170817 [9]. The lines represent predictions of a few selected EoS: purely nucleonic EoS for NS (black and solid lines), and the others (color lines) show examples of FOPT built upon nucleonic EoS considering the maximally stiff case ($c_s = c$) for the quark phase. The FOPT parameters p_{PT} (MeV fm $^{-3}$) and μ^* (MeV) are given in the inset for HS.

p versus the energy density ε . By solving the Tolman-Oppenheimer-Volkoff (TOV) equations for spherical nonrotating and nonmagnetized stellar objects [24,25], the EoS can be transformed into observational CS properties, e.g., a relation between masses and radii. For such a kind of direct comparison, it is important to accurately estimate systematic uncertainties. This can be performed for instance by solving the TOV equations for a large set of EoSs compatible with the current knowledge. In this way, the model uncertainties in the EoS can be turned into a contour in the macroscopic properties, e.g., masses, radii, and tidal deformabilities, shown in Fig. 1. The tidal deformability is well correlated to the compactness ($\beta = M/R$) of the compact star [18], and together with the measure of the mass extracted from the gravitational waveform, it allows to infer the value of the radius [20,26]. In some analyses, it is the radius prediction inferred from the tidal deformability, assuming agnostic EoS modeling or universal relations, which is directly used to select EoS models [27].

A few examples of NS and HS EoSs are shown in Fig. 1, comparing predictions based on the nucleonic SLy5 [4] (top panel) and PKDD [5] (bottom panel) EoSs. We employ in this study these two typical nucleonic EoSs which differ by the density dependence of the symmetry energy: we consider a soft nucleonic model, represented by SLy5 [4] nuclear model and a stiff nucleonic model, represented by PKDD [5] relativistic Lagrangian. The choice of reducing the nuclear EoS to only two typical ones is also performed by other authors, see for instance Ref. [28]. The SLy5 model is compatible with recent chiral effective field theory (EFT) predictions with a low value of the slope of the symmetry energy ($L_{\text{sym}} = 48.3$ MeV) [29,30], as well as with the analysis of the PREX-II experiment including also binding energies, charge radii, and dipole polarizabilities in a set of finite nuclei [31]. The stiff PKDD model ($L_{\text{sym}} = 79.5$ MeV) is compatible with another analysis of the PREX-II experiment [32].

Note that all the EoSs considered here satisfy the experimental constraints of nuclear physics, and the observations of NSs such as $2M_{\odot}$ limit, the stability, and causality conditions. Twin stars, i.e., two stars with same mass but different radii, may exist [33] but, in the present study, they are not considered since we impose a one-to-one correspondence between masses and radii.

By showing models and observational contours, Fig. 1 illustrates that it is difficult to find equations of state which reproduce equally well the contours from the NICER observatory (left panels) and from GW170817 (right panel). For instance PKDD is out of the GW170817 contour but it is in very good agreement with the two other contours from the NICER observatory. The opposite is observed for the other models which reproduce well GW170817. This tension has already been observed in previous studies, see for instance Refs. [34–37]. The mass asymmetry of the binary CS predicted for GW170817 is explored in the following analysis but we do not confirm, as suggested in Refs. [38–40], that it could resolve the mismatch illustrated in Fig. 1. Because of this tension in the data, we adopt the common strategy—we employ GW170817 to select EoSs, by comparing different kinds of binary systems: binary neutron stars (BNS), binary hybrid stars (BHS), and neutron star hybrid star (NSHS). This allows to determine whether one of these systems is favored, in a Bayesian framework, by the present data. In a second step, we combine the prediction of these modelings together with NICER contour to infer the radius $R_{1.4}$ of a $1.4M_{\odot}$ compact star.

In order to describe hybrid stars, a first order phase transition is built on top of nucleonic EoSs. The quark phase is described by the constant sound speed approach inspired from the MIT bag model [41]. It requires three quantities: the pressure p_{PT} at the entrance of the phase transition, the shift in energy density, reflecting the latent heat $\Delta\varepsilon_{PT}$, and finally, the sound speed c_s in quark matter assumed to be constant. We have [42–44]

$$\varepsilon(p) = \begin{cases} \varepsilon_{\text{NM}}(p) & p < p_{PT} \\ \varepsilon_{\text{NM}}(p_{PT}) + \Delta\varepsilon_{PT} + (p - p_{PT})/\alpha & p \geq p_{PT} \end{cases}, \quad (1)$$

where ε_{NM} is the nucleonic matter energy density, and α is related to the sound speed as $\alpha = (c_s/c)^2$, where c is the

speed of light in the vacuum. In the following, we use units where $c = 1$. A similar approach has recently been employed in [27,28,45,46], leading to the possible existence of a third branch of compact stars [47]. In our study, we use these modelings to explore the nature of CS favored by the present data.

In practice we use the parameters p_{PT} and μ^* , which represent the chemical potential of quark matter at zero pressure, and from which the latent heat $\Delta\varepsilon_{\text{PT}}$ can be recovered as

$$\Delta\varepsilon_{\text{PT}} = \frac{p_{\text{PT}}}{\alpha} \left[\frac{1 + \alpha}{\left[\frac{\mu_{\text{NM}}(p_{\text{PT}})}{\mu^*} \right]^{\frac{1+\alpha}{\alpha}} - 1} + 1 \right] - \varepsilon_{\text{NM}}(p_{\text{PT}}). \quad (2)$$

We consider the following ranges for the model parameters and we consider uniform priors: $\mu^* = 925 \pm 75$ MeV, suggested from color-superconducting quark matter calculations [48]; the sound speed parameter α is fixed to three possible values: $\alpha = 1/3$ (conformal limit), $2/3$ and 1 (causal limit); and finally, p_{PT} is an unconstrained parameter with unknown boundaries. Here, we vary p_{PT} from 6 to 500 MeV fm $^{-3}$, guided by the vanishing of the posterior distribution.

It should be noted that in the present study, quark matter may appear already around (and above) saturation density, since we explore a large space for the sound speed, ranging between $1/\sqrt{3}$ and 1 . While other analyses also explore a large space (see for instance Ref. [27]) which predict quark matter to appear on the average for densities around $1.5n_{\text{sat}}$, some analyses of quark matter predict its appearance above $3n_{\text{sat}}$ [49,50] or above $1.6M_{\odot}$ [51]. These predictions may be related to the choice of the sound speed prior, which is limited to low values in the quark phase in these analyses while we explore a wider domain in the present study.

We employ the Bayesian approach to compare our model predictions, represented by a set of EoS parameters $\{a_i\}$ with the present data [52]. The probability associated to a given model considering a set of data, the so-called the posterior probability, is

$$P(\{a_i\}|\text{data}) \sim P(\text{data}|\{a_i\}) \times P(\{a_i\}), \quad (3)$$

where $P(\text{data}|\{a_i\})$ is the likelihood function representing the ability of the model to reproduce a set of measurements and $P(\{a_i\})$ is the prior probability, which represents the *a-priori* knowledge on the model parameters. We vary the parameters controlling the FOPT, α , p_{PT} , and μ^* , which are yet unconstrained parameters. The likelihood probability entering Eq. (3) is defined as

$$P(\text{data}|\{a_i\}) = w_{\text{filter}}(\{a_i\}) \times p_{\tilde{\Lambda}}, \quad (4)$$

where $w_{\text{filter}}(\{a_i\})$ is a pass-band type filter which selects only the viable models with maximum mass larger than $2M_{\odot}$ and $p_{\tilde{\Lambda}}$ expresses the ability of the model to reproduce the observed probability density function (PDF) for $\tilde{\Lambda}$ deduced from the GW signal, considering the wave-form analysis from Refs. [9,20]. To do so, the effective tidal deformability $\tilde{\Lambda}(q)$ is averaged over the mass ratio q of the binary system in the range $[0.73, 1]$, see Ref. [35] for more details.

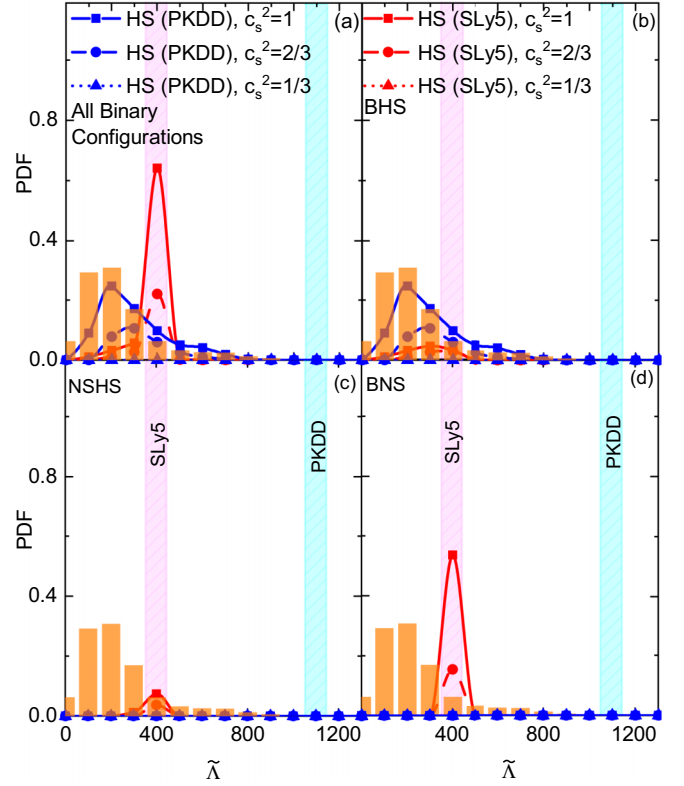


FIG. 2. Posterior PDF function of $\tilde{\Lambda}$ obtained for BNS, BHS, and NSHS configurations, compared to the data from Ref. [9]. The different line styles correspond to different sound speeds $c_s^2 = 1/3, 2/3$, and 1 . The two vertical bands represent the tidal deformabilities obtained for the purely nucleonic EoS, see the panel associated to binary configurations.

III. RESULTS AND DISCUSSION

The posterior probability as a function of the effective tidal deformability $\tilde{\Lambda}$, is shown in Fig. 2 for BNS, BHS, and NSHS configurations considering the parameter estimation from Ref. [9]. (See the Appendix for a similar figure where parameter estimation from Ref. [20] is used instead.) For BNS systems, only soft nucleonic EoS overlap the data since stiff nucleonic models predict too large tidal deformabilities. NSHS systems are not favored by either soft or stiff nucleonic EoS. Finally, BHS systems are preferred by stiff nucleonic models, overlapping at best the data, as shown in Table I where bold values mark the best overlaps. Remark that there is a non-negligible overlap of the data for BNS systems with isosoft EoS such as SLy5. It can be remarked that, in all cases, the overlap is generally optimal for large sound speed, $c_s^2 \gtrsim 2/3$, implying a stiff quark matter phase. Considering Fig. 2 and Table I, we conclude that current GW and radioastronomy observations favors stiff nucleonic EoS compatible with nuclear physics and a BHS configuration for GW170817 event. BNS configuration with soft nucleonic EoS cannot however be fully excluded.

The same EoSs are employed to predict $R_{1.4}$, as shown in Fig. 3. Independently of their ability to describe GW170817, the two nucleonic EoSs compatible with nuclear physics have

TABLE I. Overlap between the model prediction and the PDF associated to GW170817 (from Refs. [9,20]), as function of the nucleonic EoS, the sound speed in quark matter, and the nature of the binary system. The largest overlaps are stressed in bold.

	EOS	c_s^2	BHS	NSHS	BNS
soft	SLy5	1/3	0.00/0.00	0.00/0.00	0.00/0.00
	SLy5	2/3	0.07/0.07	0.04/0.04	0.07/0.07
	SLy5	1	0.12/0.15	0.08/0.08	0.06/0.07
stiff	PKDD	1/3	0.00/0.00	0.00/0.00	0.00/0.00
	PKDD	2/3	0.28/0.27	0.00/0.00	0.00/0.00
	PKDD	1	0.65/0.65	0.00/0.00	0.00/0.00

a good overlap with the NICER data for NSs: they predict radii from 12.00 km (SLy5) to 13.50 (PKDD). Table II subsumes the $R_{1,4}$ predictions conditioned by GW170817, radioastronomy and nuclear physics. We consider only the cases for which nonzero values are obtained in Table I. The centroids are weakly dependent on the nucleonic modeling, going from about 11.84 to about 12.35 km. We obtain however that the stiff nucleonic EoS, favoring the HS configuration, predicts a radius $R_{1,4} = 12.22(45)$ km, shown in Table II. The soft

TABLE II. Predictions for the $R_{1,4}$ radius constrained by both GW170817 and NICER observations of PSR J0030 + 0451, as function of the nature of the CS.

	EOS	Configuration	c_s^2	$R_{1,4}$ radius km
soft	SLy5	NS	2/3	12.00 (20)/12.00(20)
	SLy5	NS	1	12.00(20)/12.00(20)
	SLy5	HS	2/3	11.86(31)/11.97(37)
	SLy5	HS	1	11.84(32)/11.95(38)
	SLy5	HS or NS	2/3	11.98(22)/11.98(22)
	SLy5	HS or NS	1	11.96(24)/11.97(23)
	Average			11.94(31)/11.98(32)
stiff	PKDD	HS	2/3	12.06(40)/12.35(37)
	PKDD	HS	1	11.98 (39)/12.27(41)
	Average			12.02(39)/12.31(40)
	Global average			12.22(45)

nucleonic EoS, which is not favored in Table I, predicts a radius $R_{1,4} = 12.00(20)$ km. These two predictions are quite close and considering moreover their uncertainties, they are not significantly different. Let us note that the uncertainties which we report are obtained for a given nucleonic EoS. We expect, in a future work, to obtain larger uncertainties by exploring more nucleonic EoSs and therefore getting closer to the ones obtained in Refs [53,54]. We then find that the radius of a $1.4M_\odot$ CS is weakly impacted by the nucleonic EoS as well as by the nature of CS within the two nucleonic scenarios that we have investigated. By weakly, we mean that the uncertainties originating from the nucleonic EoS are not the dominant ones.

IV. CONCLUSIONS

In conclusion, we have obtained that the cross-constraints from gravitational wave, radioastronomy, x-ray observations, and nuclear physics favor binary compact star systems with stiff nucleonic EoS complemented with stiff quark matter. The neutron star-hybrid star configuration is not statistically favored for the GW170817 event. The present analysis supports the existence of $1.4 M_\odot$ mass hybrid star, with a low value for the phase transition ($n_{tr} \in [0.18, 0.35] \text{ fm}^{-3}$). Our analysis illustrates the complement between nuclear physics and astrophysics for the understanding of dense matter in CS. Future tight constraints in the slope of the symmetry energy L_{sym} will further constrain the nature of CSs in GW170817, as well as in the future astrophysical observations, such as for instance binary CS mergers, radioastronomy, or x-ray emission from millisecond pulsars.

ACKNOWLEDGMENTS

This work is supported by the Scientific and Technological Research Council of Turkey (TÜBİTAK) under Project No. MFAG-122F121 and the Yıldız Technical University under Project No. FBA-2021-4229. J.M. and E.K. are both supported by the CNRS/IN2P3 MAC project.

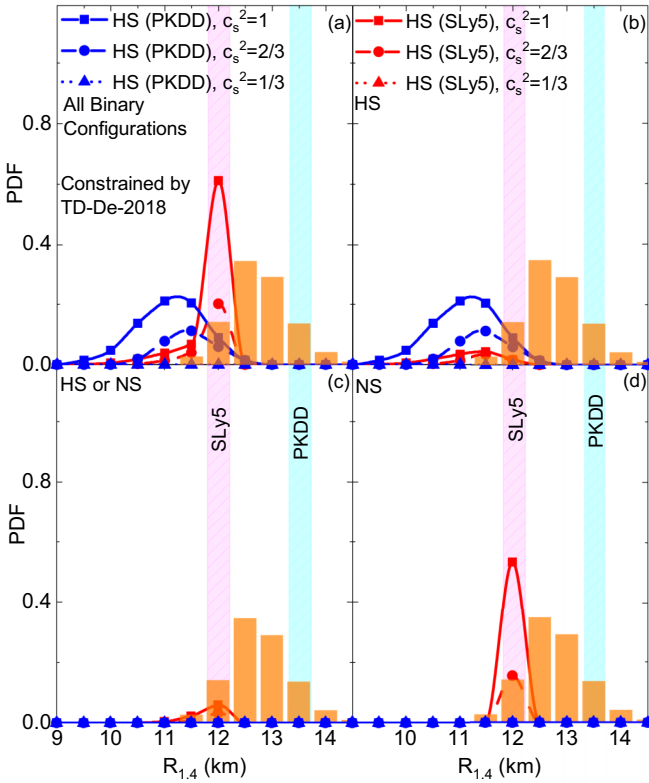


FIG. 3. Same as Fig. 2 but as function of the radius $R_{1,4}$. The data shown in the graphs are deduced from the analysis of PSR J0030 + 0451 by Miller *et al.* [7] where the PDF is sliced for masses between 1.35 and $1.45 M_\odot$. The two vertical bands represent the radii obtained from the purely nucleonic EoSs, see the panel associated to binary configurations.

APPENDIX

We provide additional figures exploring the impact of the masses in the binary system and of the distribution of the tidal deformability in our analysis.

The distributions of masses m_1 and m_2 defining the tidal deformability have been obtained in our analysis from the chirp mass $M_{\text{chirp}} = (m_1 m_2)^{3/5} m_{\text{tot}}^{-1/5}$ [20], $m_{\text{tot}} = m_1 + m_2$, and the mass fraction $q = m_1/m_2$ in the interval $[0.73-1]$ at 90% confidence level. It can also be extracted assuming a constant value of the total mass $m_{\text{tot}} = 2.73^{+0.03}_{-0.04} M_{\odot}$ independently of the mass ratio q . These two prescriptions are not totally equivalent as one can see from Fig. 4. The total mass m_{tot} is represented as function of q , where m_1 and m_2 are obtained from M_{chirp} and $q = [0.7, 1]$. Figure 4 shows that a constant value of M_{chirp} implies a nonconstant distribution of m_{tot} , which decreases by $0.05M_{\odot}$ as q varies from 0.7 up to 1. One shall indeed prefer this prescription since M_{chirp} is directly extracted from the data: M_{chirp} is the third-order post-Newtonian correction to the wavefront phase [21,23].

The fifth-order post-Newtonian correction to the wavefront phase is the tidal deformability [21,23], which is defined as

$$\tilde{\Lambda} = \frac{16}{13} \left[\frac{(m_1 + 12m_2)m_1^4}{m_{\text{tot}}^5} \Lambda_1 + 1 \leftrightarrow 2 \right]. \quad (\text{A1})$$

The impact of the two prescriptions for m_1 and m_2 into our analysis is shown in Fig. 5, where we present the posterior distribution for $R_{1,4}$ for the PKDD BHS case. The posteriors are calculated by employing the two prescriptions: a constant value for m_{tot} or a constant value for M_{chirp} . This illustrates that the small differences in the masses m_1 and m_2 obtained using one or the other of the two prescriptions have a negligible effect for our analysis.

We now analyze the impact of the extracted $\tilde{\Lambda}$ -PDF in our analysis by exploring the $\tilde{\Lambda}$ -PDF from another parameter

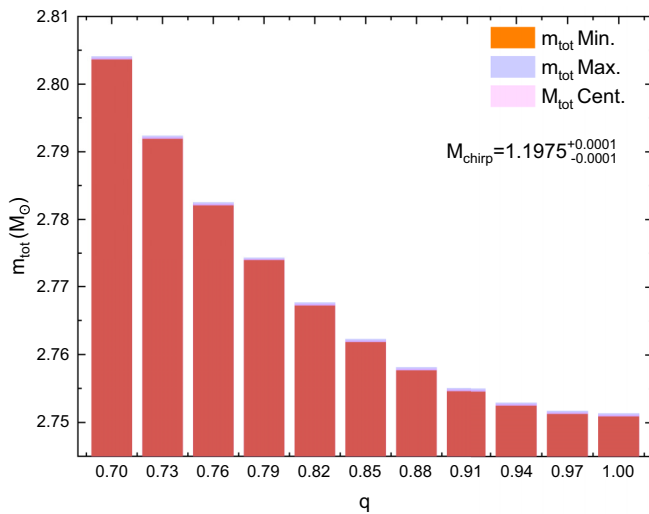


FIG. 4. The total mass m_{tot} of the binary system as function of the mass ratio q , where the chirp mass is fixed to be $M_{\text{chirp}} = 1.1975(1) M_{\odot}$ [20]. The dependence of m_{tot} in the mass ratio q shall be compared to the uncertainty in m_{tot} which is considered in the second prescription, see text for more details.

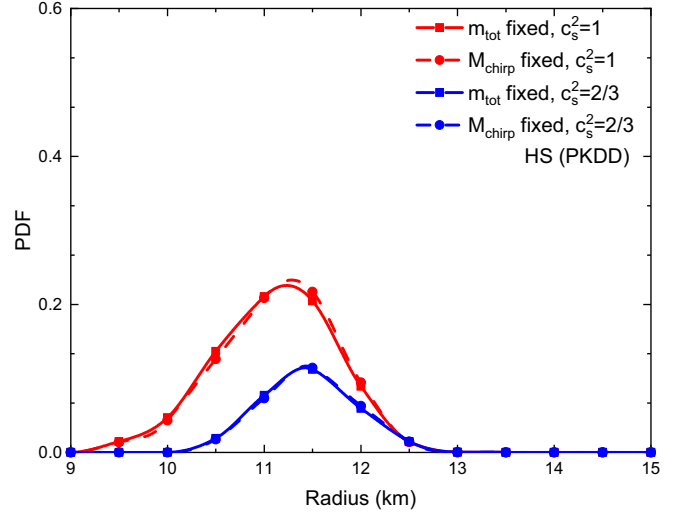


FIG. 5. Distribution of radius $R_{1,4}$ obtained with our analysis for the PKDD EoS and the BHS case, calculated using a constant value for m_{tot} (filled square symbol) or a constant value for M_{chirp} (filled circle symbol), where the data are extracted from Ref. [20]. We have considered EoS where the sound speed c_s^2 has been fixed to 1 (red lines) and to 2/3 (blue lines).

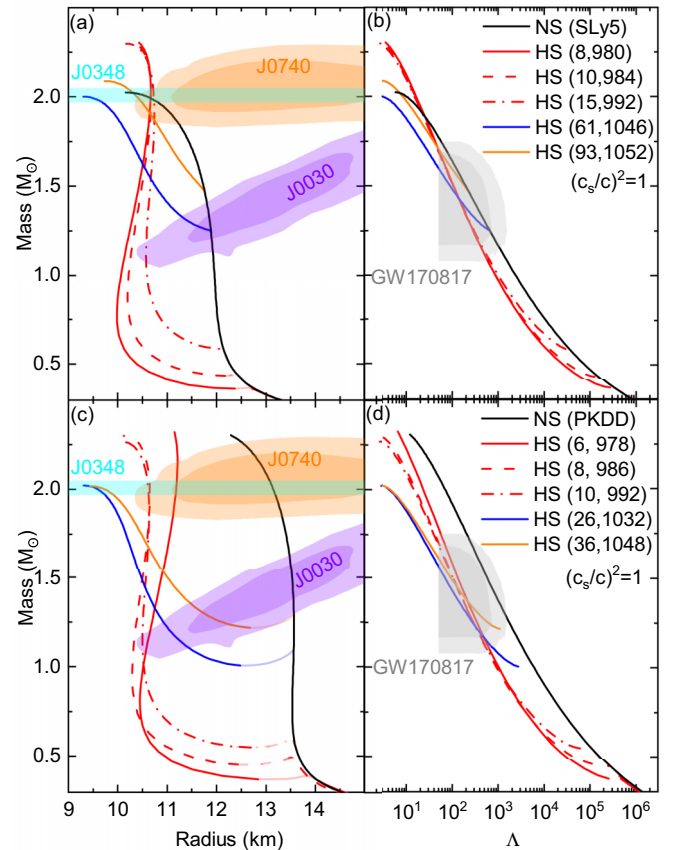


FIG. 6. Same as Fig. 1 but the contours of GW170817 are extracted from Ref. [20].

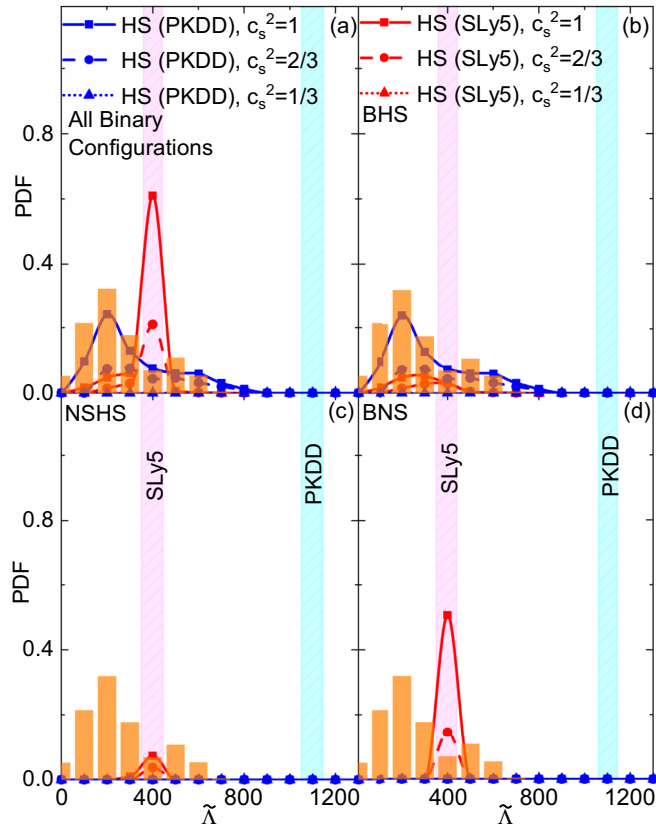
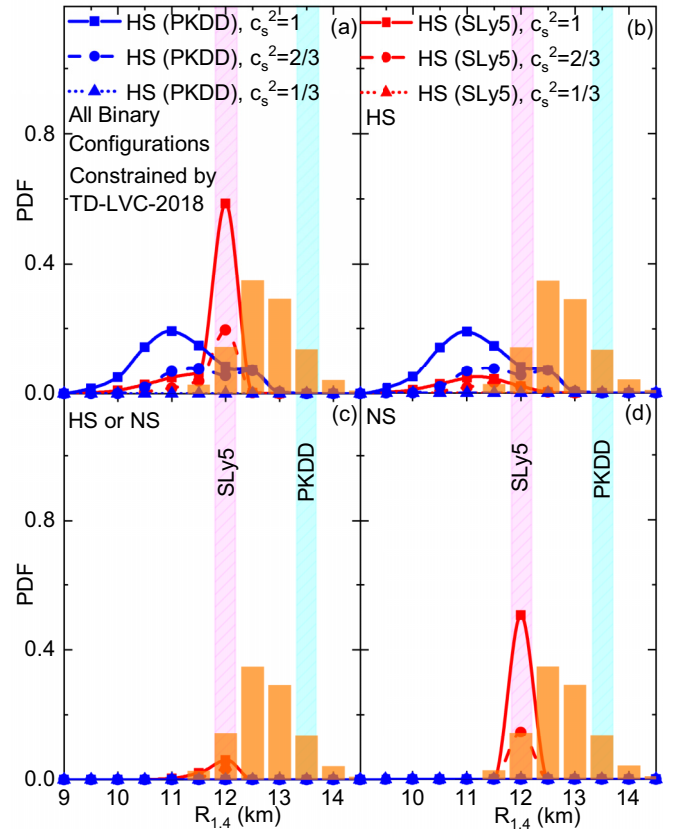


FIG. 7. Same as Fig. 2 but employing data from Ref. [20].

estimation approach. In Fig. 6, the contours of GW170817 are calculated from the prediction by the LVC [20], instead of Ref. [9], where the mass asymmetry of the binary system is given as the 1σ and 2σ confidence intervals, as in Fig. 1 of the paper. Comparing with Fig. 1 of the paper, the contour associated to GW170817 is now larger and allows a larger number of EoSs. The tension between NICER observations and GW170817 is however still visible: the EoSs compatible with the contours from the NICER observatory (PKDD for instance) have marginal overlap with the contours of GW170817.

The posterior probability as a function of the effective tidal deformability $\tilde{\lambda}$ from Ref. [20], is shown in Fig. 7 for BNS, BHS, NSHS configurations. Although, the $\tilde{\lambda}$ -PDF is qualitatively quite different between Refs. [9] (see Fig. 2 in


 FIG. 8. Same as Fig. 3 but employing the $\tilde{\lambda}$ -PDF from Ref. [20].

the paper) and [20] (with a double peaked distribution), the posteriors are almost identical between Fig. 2 the text and Fig. 7: BNS systems are preferred only with soft nuclear EoS with FOPT, NSHS systems are not favored by either soft and stiff nuclear EoS with FOPT and finally stiff nuclear EoS with FOPT is overlapping best with data for the BHS systems as shown in Table I. The overlaps are given in Table I, and they are very close.

We now come to the predictions for the radii $R_{1,4}$, using the same approach as in the paper. Results are shown in Fig. 8 where the EoSs are now constrained by $\tilde{\lambda}$ from Ref. [20]. The results are qualitatively very similar. There are however small quantitative differences which are also reported in Table II. The largest difference is of the order of 300 m.

- [1] M. G. Alford, A. Schmitt, K. Rajagopal, and T. Schäfer, Color superconductivity in dense quark matter, *Rev. Mod. Phys.* **80**, 1455 (2008).
- [2] R. Anglani, R. Casalbuoni, M. Ciminale, N. Ippolito, R. Gatto, M. Mannarelli, and M. Ruggieri, Crystalline color superconductors, *Rev. Mod. Phys.* **86**, 509 (2014).
- [3] T. H. Collaboration, Probing dense baryon-rich matter with virtual photons, *Nat. Phys.* **15**, 1040 (2019).
- [4] E. Chabanat, P. Bonche, P. Haensel, J. Meyer, and R. Schaeffer, A Skyrme parametrization from subnuclear to neutron star

densities. 2. Nuclei far from stabilities, *Nucl. Phys. A* **635**, 231 (1998); **643**, 441(E) (1998).

- [5] W. Long, J. Meng, N. VanGiai, and S.-G. Zhou, New effective interactions in relativistic mean field theory with nonlinear terms and density-dependent meson-nucleon coupling, *Phys. Rev. C* **69**, 034319 (2004).
- [6] J. Antoniadis *et al.*, A massive pulsar in a compact relativistic binary, *Science* **340**, 1233232 (2013).
- [7] M. C. Miller, F. K. Lamb, A. J. Dittmann, S. Bogdanov, Z. Arzumanyan, K. C. Gendreau, S. Guillot, A. K. Harding,

- W. C. G. Ho, J. M. Lattimer, R. M. Ludlam, S. Mahmoodifar, S. M. Morsink, P. S. Ray, T. E. Strohmayer, K. S. Wood, T. Enoto, R. Foster, T. Okajima, G. Prigozhin *et al.*, PSR j0030 + 0451 mass and radius from nicer data and implications for the properties of neutron star matter, *Astrophys. J. Lett.* **887**, L24 (2019).
- [8] M. C. Miller, F. K. Lamb, A. J. Dittmann, S. Bogdanov, Z. Arzoumanian, K. C. Gendreau, S. Guillot, W. C. G. Ho, J. M. Lattimer, M. Loewenstein, S. M. Morsink, P. S. Ray, M. T. Wolff, C. L. Baker, T. Cazeau, S. Manthripragada, C. B. Markwardt, T. Okajima, S. Pollard, I. Cognard *et al.*, The radius of PSR j0740 + 6620 from NICER and XMM-Newton data, *Astrophys. J. Lett.* **918**, L28 (2021).
- [9] S. De, D. Finstad, J. M. Lattimer, D. A. Brown, E. Berger, and C. M. Biwer, Tidal Deformabilities and Radii of Neutron Stars from the Observation of GW170817, *Phys. Rev. Lett.* **121**, 091102 (2018).
- [10] P. Demorest, T. Pennucci, S. Ransom, M. Roberts, and J. Hessels, Shapiro delay measurement of a two solar mass neutron star, *Nature (London)* **467**, 1081 (2010).
- [11] Z. Arzoumanian *et al.* (NANOGrav Collaboration), The NANOGrav 11-year data set: High-precision timing of 45 millisecond pulsars, *Astrophys. J. Suppl. Series* **235**, 37 (2018).
- [12] H. T. Cromartie *et al.*, Relativistic Shapiro delay measurements of an extremely massive millisecond pulsar, *Nat. Astron.* **4**, 72 (2019).
- [13] M. Linares, T. Shahbaz, and J. Casares, Peering into the dark side: Magnesium lines establish a massive neutron star in PSR J2215 + 5135, *Astrophys. J.* **859**, 54 (2018).
- [14] F. Özel and P. Freire, Masses, radii, and the equation of state of neutron stars, *Annu. Rev. Astron. Astrophys.* **54**, 401 (2016).
- [15] T. E. Riley *et al.*, A NICER View of PSR J0030 + 0451: Millisecond pulsar parameter estimation, *Astrophys. J. Lett.* **887**, L21 (2019).
- [16] T. E. Riley *et al.*, A NICER view of the massive pulsar PSR J0740 + 6620 informed by radio timing and XMM-Newton spectroscopy, *Astrophys. J. Lett.* **918**, L27 (2021).
- [17] K. Gendreau and Z. Arzoumanian, Searching for a pulse, *Nature Astronomy* **1**, 895 (2017).
- [18] B. P. Abbott, R. Abbott, T. D. Abbott *et al.* (LIGO Scientific Collaboration and Virgo Collaboration), GW170817: Observation of Gravitational Waves from a Binary Neutron Star Inspiral, *Phys. Rev. Lett.* **119**, 161101 (2017).
- [19] B. P. Abbott, R. Abbott, T. D. Abbott *et al.* (LIGO Scientific Collaboration and Virgo Collaboration), GW170817: Measurements of Neutron Star Radii and Equation of State, *Phys. Rev. Lett.* **121**, 161101 (2018).
- [20] B. P. Abbott, R. Abbott, T. D. Abbott *et al.* (LIGO Scientific Collaboration and Virgo Collaboration), Properties of the Binary Neutron Star Merger GW170817, *Phys. Rev. X* **9**, 011001 (2019).
- [21] E. E. Flanagan and T. Hinderer, Constraining neutron-star tidal love numbers with gravitational-wave detectors, *Phys. Rev. D* **77**, 021502(R) (2008).
- [22] T. Hinderer, Tidal love numbers of neutron stars, *Astrophys. J.* **677**, 1216 (2008).
- [23] T. Damour and A. Nagar, Relativistic tidal properties of neutron stars, *Phys. Rev. D* **80**, 084035 (2009).
- [24] R. C. Tolman, Static solutions of Einstein's field equations for spheres of fluid, *Phys. Rev.* **55**, 364 (1939).
- [25] J. R. Oppenheimer and G. M. Volkoff, On massive neutron cores, *Phys. Rev.* **55**, 374 (1939).
- [26] I. Tews, J. Margueron, and S. Reddy, Confronting gravitational-wave observations with modern nuclear physics constraints, *Eur. Phys. J. A* **55**, 97 (2019).
- [27] W.-J. Xie and B.-A. Li, Bayesian inference of the dense-matter equation of state encapsulating a first-order hadron-quark phase transition from observables of canonical neutron stars, *Phys. Rev. C* **103**, 035802 (2021).
- [28] S. Han and A. W. Steiner, Tidal deformability with sharp phase transitions in binary neutron stars, *Phys. Rev. D* **99**, 083014 (2019).
- [29] C. Drischler, K. Hebeler, and A. Schwenk, Chiral Interactions up to Next-to-Next-to-Next-to-Leading Order and Nuclear Saturation, *Phys. Rev. Lett.* **122**, 042501 (2019).
- [30] R. Somasundaram, C. Drischler, I. Tews, and J. Margueron, Constraints on the nuclear symmetry energy from asymmetric-matter calculations with chiral nn and $3n$ interactions, *Phys. Rev. C* **103**, 045803 (2021).
- [31] P.-G. Reinhard, X. Roca-Maza, and W. Nazarewicz, Information Content of the Parity-Violating Asymmetry in ^{208}Pb , *Phys. Rev. Lett.* **127**, 232501 (2021).
- [32] B. T. Reed, F. J. Fattoyev, C. J. Horowitz, and J. Piekarewicz, Implications of PREX-2 on the Equation of State of Neutron-Rich Matter, *Phys. Rev. Lett.* **126**, 172503 (2021).
- [33] J. J. Li, A. Sedrakian, and M. Alford, Ultracompact hybrid stars consistent with multimessenger astrophysics, *Phys. Rev. D* **107**, 023018 (2023).
- [34] C. D. Capano, I. Tews, S. M. Brown, B. Margalit, S. De, S. Kumar, D. A. Brown, B. Krishnan, and S. Reddy, Stringent constraints on neutron-star radii from multimessenger observations and nuclear theory, *Nat. Astron.* **4**, 625 (2020).
- [35] H. Güven, K. Bozkurt, E. Khan, and J. Margueron, Multi-messenger and multi-physics Bayesian inference for GW170817 binary neutron star merger, *Phys. Rev. C* **102**, 015805 (2020).
- [36] P. T. H. Pang, I. Tews, M. W. Coughlin, M. Bulla, C. V. D. Broeck, and T. Dietrich, Nuclear physics multimessenger astrophysics constraints on the neutron star equation of state: Adding NICER's PSR J0740 + 6620 measurement, *Astrophys. J.* **922**, 14 (2021).
- [37] H. Dinh Thi, C. Mondal, and F. Gulminelli, The nuclear matter density functional under the nucleonic hypothesis, *Universe* **7**, 373 (2021).
- [38] C. Pankow, On GW170817 and the galactic binary neutron star population, *Astrophys. J.* **866**, 60 (2018).
- [39] J. E. Horvath, The binaries of the NS-NS merging events, *AIP Conf. Proc.* **2127**, 020015 (2019).
- [40] R. Ferdman, P. Freire, B. Perera, N. Pol, F. Camilo, S. Chatterjee, J. Cordes, F. Crawford, J. Hessels, V. Kaspi *et al.*, Asymmetric mass ratios for bright double neutron-star mergers, *Nature (London)* **583**, 211 (2020).
- [41] A. Chodos, R. L. Jaffe, K. Johnson, C. B. Thorn, and V. F. Weisskopf, New extended model of hadrons, *Phys. Rev. D* **9**, 3471 (1974).
- [42] J. L. Zdunik and P. Haensel, Maximum mass of neutron stars and strange neutron-star cores, *Astron. Astrophys.* **551**, A61 (2013).
- [43] M. G. Alford, S. Han, and M. Prakash, Generic conditions for stable hybrid stars, *Phys. Rev. D* **88**, 083013 (2013).

- [44] N. Chamel, A. F. Fantina, J. M. Pearson, and S. Goriely, Phase transitions in dense matter and the maximum mass of neutron stars, *Astron. Astrophys.* **553**, A22 (2013).
- [45] R. Somasundaram and J. Margueron, Impact of massive neutron star radii on the nature of phase transitions in dense matter, *Europhys. Lett.* **138**, 14002 (2022).
- [46] R. Somasundaram, I. Tews, and J. Margueron, Investigating signatures of phase transitions in neutron-star cores, *Phys. Rev. C* **107**, 025801 (2023).
- [47] M. Alford and A. Sedrakian, Compact Stars with Sequential QCD Phase Transitions, *Phys. Rev. Lett.* **119**, 161104 (2017).
- [48] B. K. Agrawal, Equations of state and stability of color-superconducting quark matter cores in hybrid stars, *Phys. Rev. D* **81**, 023009 (2010).
- [49] A. Pfaff, H. Hansen, and F. Gulminelli, Bayesian analysis of the properties of hybrid stars with the Nambu–Jona-Lasinio model, *Phys. Rev. C* **105**, 035802 (2022).
- [50] A. Ayriyan, D. Alvarez-Castillo, D. Blaschke, and H. Grigorian, Bayesian analysis for extracting properties of the nuclear equation of state from observational data including tidal deformability from GW170817, *Universe* **5**, 61 (2019).
- [51] A. Parisi, C. V. Flores, C. H. Lenzi, C.-S. Chen, and G. Lugones, Hybrid stars in the light of the merging event GW170817, *J. Cosmol. Astropart. Phys.* **06** (2021) 042.
- [52] A. W. Steiner, Moving beyond chi-squared in nuclei and neutron stars, *J. Phys. G: Nucl. Part. Phys.* **42**, 034004 (2015).
- [53] T. Dietrich, M. W. Coughlin, P. T. H. Pang, M. Bulla, J. Heinzel, L. Issa, I. Tews, and S. Antier, Multimessenger constraints on the neutron-star equation of state and the hubble constant, *Science* **370**, 1450 (2020).
- [54] M. Al-Mamun, A. W. Steiner, J. Nättilä, J. Lange, R. O’Shaughnessy, I. Tews, S. Gandolfi, C. Heinke, and S. Han, Combining Electromagnetic and Gravitational-Wave Constraints on Neutron-Star Masses and Radii, *Phys. Rev. Lett.* **126**, 061101 (2021).